Geometry Preprint 201 (2009), Vienna University of Technology

A kinematic approach to Kokotsakis meshes

Hellmuth Stachel[1]

Institute of Discrete Mathematics and Geometry, Vienna University of Technology, Wiedner Hauptstr. 8-10/104, A 1040 Wien, Austria

Abstract

A Kokotsakis mesh is a polyhedral structure consisting of an n-sided central polygon $\mathcal{P}_0$ surrounded by a belt of polygons in the following way: Each side a_i of $\mathcal{P}_0$ is shared by an adjacent polygon $\mathcal{P}_i$, and the relative motion between cyclically consecutive neighbor polygons is a spherical coupler motion. Hence, each vertex of $\mathcal{P}_0$ is the meeting point of four faces. In the case $n = 3$ the mesh is part of an octahedron.

These structures with rigid faces and variable dihedral angles were first studied in the thirties of the last century. However, in the last years there was a renaissance: The question under which conditions such meshes are infinitesimally or continuously flexible gained high actuality in discrete differential geometry. The goal of this paper is to revisit the wellknown continuously flexible examples (Bricard, Graf, Sauer, Kokotsakis) from the kinematic point of view and to extend their list by a new family.

Keywords: Kokotsakis mesh, discrete conjugate net, overconstrained mechanism, spherical coupler motion

1. Introduction

The definition of a Kokotsakis mesh (German: Neunflach) dates back to A.I. Kokotsakis (1932). While for arbitrary n the classification of *continously flexible* Kokotsakis meshes is an open problem (compare Bobenko et al., 2008, p. 76), for the case $n = 3$ we know since R. Bricard (1897) that there are three flexible types (see also Stachel, 1987).

In discrete differential geometry there is an interest in polyhedral structures composed of quadrilaterals, i.e., in *quadrilateral surfaces*. When all quadrilaterals are planar, the edges form a *discrete conjugate net* (see, e.g., Pottmann et al., 2007, Fig. 14e). When each quadrilateral is seen as a rigid body and only the dihedral angles can vary, the question arises under which conditions such structures are flexible. In Bobenko et al. (2008), p. 75, the following theorem

[1] *Email address:* stachel@dmg.tuwien.ac.at,
URL: http://www.dmg.tuwien.ac.at/stachel

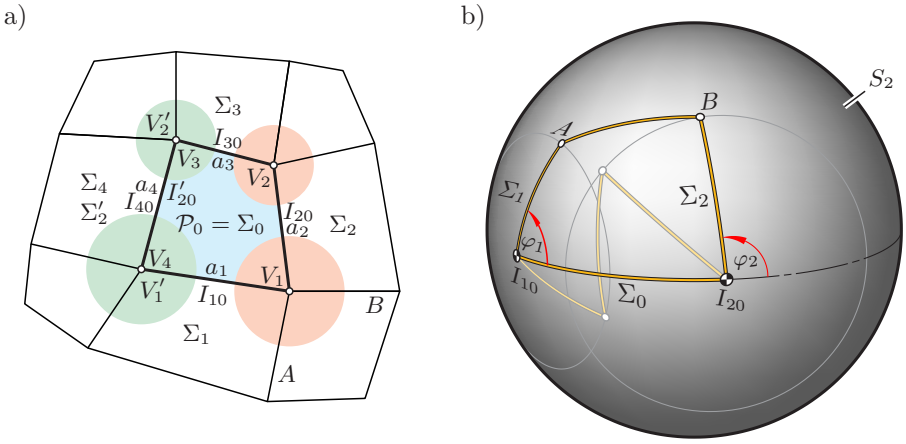

Figure 1: a) Kokotsakis mesh for $n = 4$ and b) spherical image of the pyramide with apex V_1

can be found:

A discrete conjugate net is continuously flexible if and only if all its 3×3 complexes, i.e., all included Kokotsakis meshes, are continuously flexible.

This reveals the recent interest in these examples of overconstrained structures.

1.1. Kinematic interpretation

Let us concentrate on the case $n = 4$ (see Fig. 1a). In terms of kinematics the involved polygons $\mathcal{P}_0, \ldots, \mathcal{P}_4$ represent different *systems* $\Sigma_0, \ldots, \Sigma_4$, i.e., rigid bodies. The central polygon $\mathcal{P}_0$ with vertices $V_1, \ldots, V_3$ and sides $a_1, \ldots, a_4$ stands for the fixed system Σ_0. The sides a_i are instantaneous axes I_{i0} of the relative motions Σ_i/Σ_0, i.e., of Σ_i against Σ_0.

For $n = 4$ the edges of a Kokotsakis mesh constitute a net of *folds*. There are four connected triples of edges. For the sake of brevity, we call them *horizontal* or *vertical* (note Fig. 1a). The horizontal folds include either a_1 or a_3 as central edge, the vertical folds pass either through a_2 or through a_4. Each vertex V_i is a crossing point of a horizontal and a vertical fold.

Since not the lengths of the sides $a_1 = \overline{V_1V_2}, \ldots, a_4 = \overline{V_4V_1}$ of $\mathcal{P}_0$, but only their directions have an influence on the flexibility, we can translate all four-sided pyramides with apex V_i, $i = 1, \ldots, 4$, through a common center O. If we intersect these pyramides with the unit sphere S_2 centered at O, we obtain the *spherical image* of the mesh. Then we can state:

Theorem 1. *A Kokotsakis mesh is of k-th order infinitesimally flexible, $k = 1, 2, \ldots$, or continuously flexible if and only if its spherical image is of k-th order infinitesimally or continuously flexible, respectively.*

First order infinitesimal flexibility of such meshes has been characterized by Kokotsakis (1932) and recently by O.N. Karpenkov (2008). It should be noted that due to B. Wegner (1984) first order flexibility of a spherical structure is

equivalent to first order flexibility of its planar sections; this principle called 'coning' is the main reason for the projective invariance of first order flexibility. 2nd order infinitesimal flexibility or Kokotsakis meshes has recently been studied in Bobenko et al. (2008).

If we intersect the planes adjacent to the vertex V_i with a sphere centered at V_i, the relative motion Σ_{i+1}/Σ_i, $i = 1, \dots, 4 \pmod 4$, is a spherical coupler motion. To recall, a *spherical coupler motion* (see Fig. 1b) is based on a spherical quadrangle $I_{10}I_{20}BA$ with constant edge lengths but variable angles. It transmits the rotation about the center I_{10} through the angle φ_1 by the coupler AB non-uniformly to the rotation about I_{20} through φ_2.

A Kokotsakis mesh is continuously flexible if and only if the transmission of the rotation Σ_1/Σ_0 to Σ_3/Σ_0 by the two coupler motions at V_1 and V_2 on the right hand side (Fig. 1a) is the same as via V_4 and V_3 on the left hand side. This is why we change the notation slightly and replace $\Sigma_4, V_4, V_3, a_4 = I_{40}$ by $\Sigma_2', V_1', V_2', a_2' = I_{20}'$, respectively. Of course, in the flexible case there is also a two-fold 'horizontal' decomposition of the transmission Σ_2'/Σ_2, one via Σ_1 and the other via Σ_3.

The transference from a Kokotsakis mesh to its spherical image gives a unique result only if each edge is oriented. It is quite natural to endow the axes $I_{10}, \dots, I_{40}$ with an orientation since the angles of rotations about these axes need to be signed. However, the orientation of all other edges — or, equivalently, the choice of half-edges terminated by V_i — is arbitrary. This leads to some ambiguities.

1.2. Known continously flexible examples

Up to recent, to the author's best knowledge the following examples of continuously flexible Kokotsakis meshes are known. Under appropriate notation and orientation of edges the flexible cases can be characterized as follows:

(I) **Planar-symmetric** type (Kokotsakis, 1932, § 18): The reflection in the plane of symmetry of V_1 and V_4 maps each horizontal fold onto itself while the two vertical folds are exchanged.

(II) **Translational** type: There is a translation $V_1 \mapsto V_4$ and $V_2 \mapsto V_3$ mapping the three planes on the right hand side onto the triple on the left hand side.

(III) **Isogonal** type (Kokotsakis, 1932; Bobenko et al., 2008): At each vertex opposite angles are congruent. We return to this 3×3 complex of a Voss surface in Section 4.1.

(IV) **Orthogonal** type (Sauer, Graf, 1931; Sauer, 1970): Here the horizontal folds are located in parallel (say: horizontal) planes, the vertical folds in vertical planes. $\mathcal{P}_0$ is a trapezoid. The underlying conditions for this 3×3 complex of T-nets will be presented in Section 4.2.

In Section 4.3 a new family of continuously flexible Kokotsakis meshes will be introduced, which we call the **line-symmetric** type V though the symmetries

are only locally. This family includes Kokotsaki's remarkable example of a planar tesselation with congruent convex quadrangles (Kokotsakis (1932, Fig. 15), note also Bobenko et al. (2008, Fig. 8) or Stachel (2009)).

The famous Miura-ori folding technique (e.g., Piekarski (2000) or Stachel (2009)) contains 3×3 complexes which are of type II, III and IV, simultaneously. As shown in Stachel (2000), any Cardan joint is also based on a spherical coupler motion, however a particular case where the sides $I_{10}A$, $I_{20}B$ and AB have the spherical length $\pi/2$. An appropriate combination of two Cardan joints gives a uniform transmission from Σ_1 to Σ_3. This results in a flexible case with parallel axes I_{10} and I_{30} which obeys the conditions of type V; however, the second decomposition according to type V is no more a Cardan joint.

We finally emphasize that the complete classification of continuously flexible meshes has not been achieved yet.

1.3. Conventions

According to Theorem 1 our investigation takes place on the unit sphere S^2 with center O. In order to avoid ambiguities in spherical geometry, we introduce the following notations and conventions:

- Each point A on the sphere has a diametrically opposed point $\overline{A}$, its *antipode*. A circle on S^2 passing through A is a *great circle* if and only if it passes also through $\overline{A}$.
- For any two points A, B with $B \neq A, \overline{A}$ the *spherical segment* or *bar* AB stands for the shorter of the two connecting arcs on the great circle spanned by A and B. We denote this great circle by $[AB]$.
- The *spherical distance* $\overline{AB}$ is defined as the arc length of the segment AB. We require $0 \leq \overline{AB} \leq \pi$ thus including also the limiting cases $B = A$ and $B = \overline{A}$.
- The *oriented angle* $\sphericalangle ABC$ on S^2 is the angle of the rotation about axis OB which carries the segment BA into a position aligned with the segment BC. This angle is oriented in the mathematical sense, if looking from outside, and can be bounded by $-\pi < \sphericalangle ABC \leq \pi$.

2. Analysis of a spherical coupler motion

We start with the analysis of the spherical coupler motion, which is the spherical image of the flexing pyramide with apex V_1 (Fig. 2): Let $I_{10}I_{20}$ be the frame link of a spherical four-bar with the coupler A_1B_1. We denote the spherical length of the driving arm $I_{10}A_1$ with α_1 and that of the driven arm $I_{20}B_1$ with β_1. Furthermore, we set $\gamma_1 := \overline{A_1B_1}$ and $\delta_1 := \overline{I_{10}I_{20}}$ obeying

$$0 < \alpha_1, \beta_1, \gamma_1, \delta_1 < \pi\,.$$

The movement of the coupler remains unchanged when A_1 is replaced by its antipode $\overline{A}_1$ and at the same time α_1 and γ_1 are substituted by $\pi - \alpha_1$ and

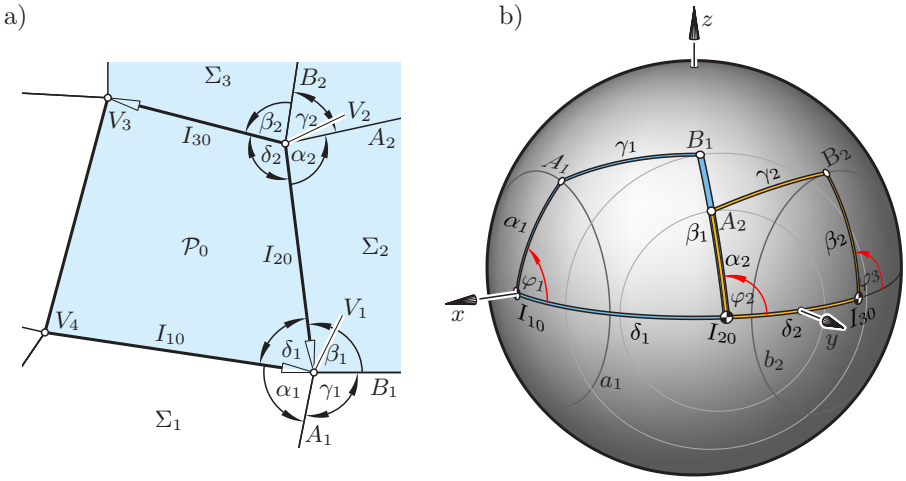

Figure 2: a) Pyramides with apices V_1 and V_2 and b) composition of the two spherical four-bars $I_{10}A_1B_1I_{20}$ and $I_{20}A_2B_2I_{30}$ with side lengths $\alpha_i, \beta_i, \gamma_i, \delta_i$, $i = 1, 2$

$\pi - \delta_1$, respectively. The same holds for the other vertices. When I_{10} is replaced by its antipode $\overline{I}_{10}$, then also the sense of orientation changes, when the rotation of the driving bar $I_{10}A_1$ is inspected from outside of S^2 either at I_{10} or at $\overline{I}_{10}$.

2.1. Relation between input and output angle

We use a cartesian coordinate frame with I_{10} on the positive x-axis and $I_{10}I_{20}$ in the xy-plane such that I_{20} has a positive y-coordinate (see Fig. 2b). The input angle φ_1 is measured between $I_{10}I_{20}$ and the driving arm $I_{10}A_1$ in mathematically positive sense. The output angle φ_2 is the oriented exterior angle at vertex I_{20}, hence $\varphi_2 = \sphericalangle \overline{I}_{10}I_{20}B_1$. This results in the following coordinates:

$$A_1 = \begin{pmatrix} \mathrm{c}\alpha_1 \\ \mathrm{s}\alpha_1\,\mathrm{c}\varphi_1 \\ \mathrm{s}\alpha_1\,\mathrm{s}\varphi_1 \end{pmatrix} \text{ and } \quad B_1 = \begin{pmatrix} \mathrm{c}\beta_1\,\mathrm{c}\delta_1 - \mathrm{s}\beta_1\,\mathrm{s}\delta_1\,\mathrm{c}\varphi_2 \\ \mathrm{c}\beta_1\,\mathrm{s}\delta_1 + \mathrm{s}\beta_1\,\mathrm{c}\delta_1\,\mathrm{c}\varphi_2 \\ \mathrm{s}\beta_1\,\mathrm{s}\varphi_2 \end{pmatrix}.$$

Herein s and c are abbreviations for the sine and cosine function, respectively. In these equations the lengths α_1, β_1 and δ_1 are signed. The coordinates would also be valid for negative lengths.

The constant length γ_1 of the coupler implies the condition

$$\begin{aligned} &\mathrm{c}\alpha_1\,\mathrm{c}\beta_1\,\mathrm{c}\delta_1 - \mathrm{c}\alpha_1\,\mathrm{s}\beta_1\,\mathrm{s}\delta_1\,\mathrm{c}\varphi_2 + \mathrm{s}\alpha_1\,\mathrm{c}\beta_1\,\mathrm{s}\delta_1\,\mathrm{c}\varphi_1 \\ &+ \mathrm{s}\alpha_1\,\mathrm{s}\beta_1\,\mathrm{c}\delta_1\,\mathrm{c}\varphi_1\,\mathrm{c}\varphi_2 + \mathrm{s}\alpha_1\,\mathrm{s}\beta_1\,\mathrm{s}\varphi_1\,\mathrm{s}\varphi_2 = \mathrm{c}\gamma_1. \end{aligned} \tag{1}$$

Now we express $\mathrm{s}\varphi_i$ and $\mathrm{c}\varphi_i$ in terms of $t_i := \tan\varphi_i/2$ setting

$$\mathrm{c}\varphi = \frac{1 - t_i^2}{1 + t_i^2}, \quad \mathrm{s}\varphi = \frac{2t_i}{1 + t_i^2}.$$

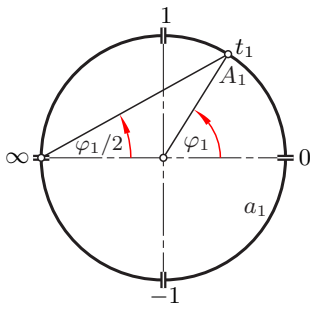

Figure 3: $t_1 = \tan\varphi_1/2$ is a projective coordinate of point A_1 on the circle a_1

Note that t_1 is a *projective coordinate* of point A_1 on the circle a_1 (see Fig. 3). The same is true for t_2 and $B_1 \in b_1$. From (1) we obtain

$$\begin{aligned} &\mathrm{c}\alpha_1\,\mathrm{c}\beta_1\,\mathrm{c}\delta_1 - \mathrm{c}\alpha_1\,\mathrm{s}\beta_1\,\mathrm{s}\delta_1\,\frac{1-t_2^2}{1+t_2^2} + \mathrm{s}\alpha_1\,\mathrm{c}\beta_1\,\mathrm{s}\delta_1\,\frac{1-t_1^2}{1+t_1^2} \\ &+ \mathrm{s}\alpha_1\,\mathrm{s}\beta_1\,\mathrm{c}\delta_1\,\frac{1-t_1^2}{1+t_1^2}\,\frac{1-t_2^2}{1+t_2^2} + \mathrm{s}\alpha_1\,\mathrm{s}\beta_1\,\frac{2t_1}{1+t_1^2}\,\frac{2t_2^2}{1+t_2^2} = \mathrm{c}\gamma_1 \end{aligned}$$

or

$$\begin{aligned} -K(1+t_1^2)(1-t_2^2) + L(1-t_1^2)(1+t_2^2) + M(1-t_1^2)(1-t_2^2) \\ + 4\,\mathrm{s}\alpha_1\,\mathrm{s}\beta_1\,t_1t_2 + N(1+t_1^2)(1+t_1^2) = 0\,, \end{aligned} \tag{2}$$

where

$$\begin{aligned} K &= \mathrm{c}\alpha_1\,\mathrm{s}\beta_1\,\mathrm{s}\delta_1\,, \qquad M = \mathrm{s}\alpha_1\,\mathrm{s}\beta_1\,\mathrm{c}\delta_1\,, \\ L &= \mathrm{s}\alpha_1\,\mathrm{c}\beta_1\,\mathrm{s}\delta_1\,, \qquad N = \mathrm{c}\alpha_1\,\mathrm{c}\beta_1\,\mathrm{c}\delta_1 - \mathrm{c}\gamma_1\,. \end{aligned} \tag{3}$$

The biquadratic equation (2) describes a *2-2-correspondence* between points A_1 on circle $a_1 = (I_{10}; \alpha_1)$ and B_1 on $b_1 = (I_{20}; \beta_1)$. It can be abbreviated by

$$c_{22}t_1^2t_2^2 + c_{20}t_1^2 + c_{02}t_2^2 + c_{11}t_1t_2 + c_{00} = 0 \tag{4}$$

setting

$$\begin{aligned} c_{00} &= -K + L + M + N, \qquad c_{02} = K + L - M + N, \\ c_{11} &= 4\,\mathrm{s}\alpha_1\,\mathrm{s}\beta_1 \neq 0\,, \\ c_{20} &= -K - L - M + N, \qquad c_{22} = K - L + M + N\,. \end{aligned} \tag{5}$$

Alternatively, (2) can also be expressed as

$$\begin{aligned} &\sin\frac{\alpha_1-\beta_1+\gamma_1+\delta_1}{2}\,\sin\frac{\alpha_1-\beta_1-\gamma_1+\delta_1}{2}\,t_1^2t_2^2 \\ &+ \sin\frac{\alpha_1+\beta_1+\gamma_1+\delta_1}{2}\,\sin\frac{\alpha_1+\beta_1-\gamma_1+\delta_1}{2}\,t_1^2 - 2\,\sin\alpha_1\,\sin\beta_1\,t_1t_2 \\ &+ \sin\frac{\alpha_1+\beta_1+\gamma_1-\delta_1}{2}\,\sin\frac{\alpha_1+\beta_1-\gamma_1-\delta_1}{2}\,t_2^2 \\ &+ \sin\frac{\alpha_1-\beta_1+\gamma_1-\delta_1}{2}\,\sin\frac{\alpha_1-\beta_1-\gamma_1-\delta_1}{2} = 0\,. \end{aligned} \tag{6}$$

Remark: It should be noted that conversely the 2-2-correspondance (4) defines $\alpha_1, \ldots, \delta_1$ uniquely. This can be seen as follows: First we get

$$\begin{aligned} 4K &= -c_{00} + c_{02} - c_{20} + c_{22}\,, \quad 4L = c_{00} + c_{02} - c_{20} - c_{22}\,, \\ 4M &= c_{00} - c_{02} - c_{20} + c_{22}\,, \quad 4N = c_{00} + c_{02} + c_{20} + c_{22}\,. \end{aligned}$$

On the other hand

$$\frac{4K}{c_{11}} = \frac{\mathrm{s}\delta_1}{\tan\alpha_1}\,, \quad \frac{4L}{c_{11}} = \frac{\mathrm{s}\delta_1}{\tan\beta_1}\,, \quad \frac{4M}{c_{11}} = \mathrm{c}\delta_1\,, \quad \frac{4N}{c_{11}} = \frac{\mathrm{c}\alpha_1\,\mathrm{c}\beta_1\,\mathrm{c}\delta_1 - \mathrm{c}\gamma}{\mathrm{s}\alpha_1\,\mathrm{s}\beta_1}\,.$$

This gives consecutively $\mathrm{c}\delta_1$, $\tan\alpha_1$, $\tan\beta_1$ and $\mathrm{c}\gamma_1$, which defines the four bar-lengths uniquely within the intervall $[0,\pi]$.

2.2. Relation between opposite angles

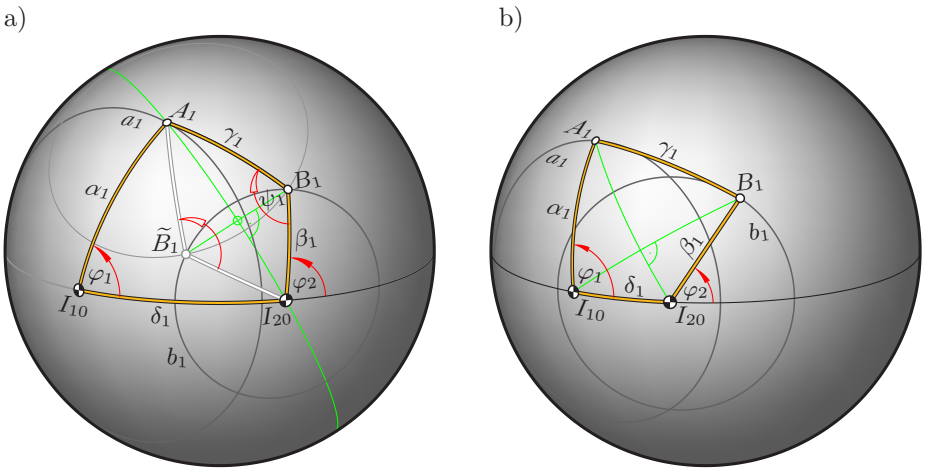

Figure 4: a) Opposite angles φ_1 and ψ_1 at the spherical four-bar $I_{10}A_1B_1I_{20}$; b) Orthogonal case: each quadrangle has orthogonal diagonals

At the end of this analysis of a spherical four-bar mechanism we focus on opposite angles in the spherical quadrangle $I_{10}A_1B_1I_{20}$: The diagonal A_1I_{20} splits the quadrangle into two triangles, and we inspect the interior angles φ_1 at I_{10} and ψ_1 at B_1 (Fig. 4a). Also for non-convex quadrangles, the spherical Cosine Theorem implies

$$\cos\overline{A_1I_{20}} = \mathrm{c}\beta_1\,\mathrm{c}\gamma_1 + \mathrm{s}\beta_1\,\mathrm{s}\gamma_1\,\mathrm{c}\psi_1 = \mathrm{c}\alpha_1\,\mathrm{c}\delta_1 + \mathrm{s}\alpha_1\,\mathrm{s}\delta_1\,\mathrm{c}\varphi_1$$

Hence there is a linear function, i.e., there are constants $k_1, l_1 \in \mathbb{R}$ such that

$$\mathrm{c}\psi_1 = k_1 + l_1\mathrm{c}\varphi_1 \quad \text{for} \quad -1 \le \mathrm{c}\psi_1, \mathrm{c}\varphi_1 \le 1 \tag{7}$$

with

$$k_1 = \frac{\mathrm{c}\alpha_1\,\mathrm{c}\delta_1 - \mathrm{c}\beta_1\,\mathrm{c}\gamma_1}{\mathrm{s}\beta_1\,\mathrm{s}\gamma_1}\,, \quad l_1 = \frac{\mathrm{s}\alpha_1\,\mathrm{s}\delta_1}{\mathrm{s}\beta_1\,\mathrm{s}\gamma_1}\,. \tag{8}$$

For later use it is necessary to define also ψ_1 as an oriented angle, hence

$$\psi_1 = \sphericalangle I_{20}B_1A_1, \quad \varphi_1 = \sphericalangle I_{20}I_{10}A_1 \quad \text{under} \quad -\pi < \psi_1, \varphi_1 \le \pi\,.$$

This is still compatible with eq. (7).

We note that in general for given φ_1 there are two positions B_1 and $\widetilde{B}_1$ on circle b_1 obeying (7). They are placed symmetrically with respect to the diagonal A_1I_{20}. So, the corresponding oriented angles $\sphericalangle I_{20}B_1A_1$ and $\sphericalangle I_{20}\widetilde{B}_1A_1$ have different signs (Fig. 4a).

Lemma 2. *The cosines of the opposite oriented angles $\psi_1 = \sphericalangle I_{20}B_1A_1$ and $\varphi_1 = \sphericalangle I_{20}I_{10}A_1$ at the four-bar are linearly related by eq. (7). The signs of φ_1 and ψ_1 are different if and only if B_1 and I_{10} are on different sides of $[A_1I_{20}]$.*

Remark: Contrary to the 2-2-correspondance describing the relation between φ_1 and φ_2, the linear function (7) does not characterize the underlying four-bar uniquely. This follows immediately from a parameter count.

2.3. Particular cases

Spherical isogram:

Under the conditions $\beta_1 = \alpha_1$ and $\delta_1 = \gamma_1$ opposite sides of the quadrangle $I_{10}A_1B_1I_{20}$ have equal lengths. Such quadrangles are called spherical *isograms*. In this case we have $c_{00} = c_{22} = 0$ in (4), and eq. (6) converts into

$$\mathrm{s}\alpha_1 \left[-2\,\mathrm{s}\alpha_1\, t_1t_2 + \mathrm{s}(\alpha_1+\gamma_1)\, t_1^2 + \mathrm{s}(\alpha_1-\gamma_1)\, t_2^2\right] = 0.$$

The left hand side can be decomposed as

$$\begin{aligned}&\mathrm{s}(\alpha_1-\gamma_1)\left[\mathrm{s}(\alpha_1-\gamma_1)\, t_2^2 - 2\,\mathrm{s}\alpha_1\, t_1t_2 + \mathrm{s}(\alpha_1+\gamma_1)\, t_1^2\right]\\ &= \left[\mathrm{s}(\alpha_1-\gamma_1)t_2 - (\mathrm{s}\alpha_1+\mathrm{s}\gamma_1)t_1\right]\left[\mathrm{s}(\alpha_1-\gamma_1)t_2 - (\mathrm{s}\alpha_1-\mathrm{s}\gamma_1)t_1\right]\end{aligned}$$

because of $\mathrm{s}^2\alpha_1 - \mathrm{s}^2\gamma_1 = \mathrm{s}(\alpha_1+\gamma_1)\,\mathrm{s}(\alpha_1-\gamma_1)$. *The 2-2-correspondance* between the circles a_1 and b_1 *splits into two projectivities*[2]

$$t_1 \;\mapsto\; t_2 = \frac{(\mathrm{s}\alpha_1 \pm \mathrm{s}\gamma_1)}{\mathrm{s}(\alpha_1-\gamma_1)}\, t_1\,, \tag{9}$$

provided $\alpha_1 \neq \gamma_1,\ \pi-\gamma_1$. Both projectivities keep $t_1 = 0$ and $t_1 = \infty$ fixed (Fig. 3). These parameters belong to the two *folded* positions, where the coupler A_1B_1 is aligned with the frame link $I_{10}I_{20}$. In these positions a bifurcation is possible between the two projectivities. (Note that at the planar analogue one of these projectivities is the identity $t_2 = t_1$ as $I_{10}A_1B_1I_{20}$ is a parallelogram.)

Orthogonal case:

For a given point $A_1 \in a_1$ the corresponding $B_1, \widetilde{B}_1 \in b_1$ are the points of intersection between the circles $(A_1;\gamma_1)$ and $b_1 = (I_{20};\beta_1)$ (see Fig. 4a). Hence, B_1 and $\widetilde{B}_1$ are located on a great circle perpendicular to the great circle $[A_1I_{20}]$.

[2] As mentioned above, the vertices of the moving quadrangle can be replaced by their antipodes whithout changing the motion. This is the reason why the same property also shows up under $\beta_1 = \pi-\alpha_1$ and $\delta_1 = \pi-\gamma_1$. We will not mention this in the future but only refer to an 'appropriate choice of orientations'.

Under the condition

$$\cos\alpha_1\,\cos\beta_1 = \cos\gamma_1\,\cos\delta_1. \tag{10}$$

the diagonals of the spherical quadrangle $I_{10}A_1B_1I_{20}$ are orthogonal (Fig. 4b) as each of the products equals the products of cosines of the four segments on the two diagonals. Hence, under (10) B_1 and $\widetilde{B}_1$ are always aligned with I_{10}, but also conversely, the two points A_1 and $\widetilde{A}_1$ corresponding to B_1 are aligned with I_{20}.

Lemma 3. *Under condition (10) the 2-2-correspondence between a_1 and b_1 maps pairs of points $A_1 \in a_1$ spherically aligned with I_{20} onto pairs of points $B_1 \in b_1$ which are spherically aligned with I_{10}. Corresponding great circles $[I_{20}A_1]$ and $[I_{10}B_1]$ are orthogonal (Fig. 4b).*

Remark: In the notation (4) this is characterized by $\det\begin{pmatrix} c_{22} & c_{02} \\ c_{20} & c_{00} \end{pmatrix} = 0$, because by (5) this is equivalent to $\det\begin{pmatrix} K & N \\ M & -L \end{pmatrix} = 0$, which means

$$\mathrm{s}\alpha_1\,\mathrm{c}\alpha_1\,\mathrm{s}\beta_1\,\mathrm{c}\beta_1\,\mathrm{s}^2\delta_1 + \mathrm{s}\alpha_1\,\mathrm{c}\alpha_1\,\mathrm{s}\beta_1\,\mathrm{c}\beta_1\,\mathrm{c}^2\delta_1 - \mathrm{s}\alpha_1\,\mathrm{s}\beta_1\,\mathrm{c}\gamma_1\,\mathrm{c}^2\delta_1 = 0$$

or

$$\mathrm{s}\alpha_1\,\mathrm{c}\alpha_1\,\mathrm{s}\beta_1\,\mathrm{c}\beta_1 = \mathrm{s}\alpha_1\,\mathrm{s}\beta_1\,\mathrm{c}\gamma_1\,\mathrm{c}\delta_1 \quad \text{under} \quad \mathrm{s}\alpha_1\,\mathrm{s}\beta_1 \neq 0\,.$$

3. Composition of two spherical coupler motions

Now we use the output angle φ_2 of this coupler motion as the input angle of a second coupler motion with vertices $I_{20}A_2B_2I_{30}$, with arm lengths α_2, β_2, with the coupler length γ_2 and with δ_2 as length of the frame link (Fig. 2b). The two frame links are assumed in aligned position. In the case $\sphericalangle I_{10}I_{20}I_{30} = \pi$ the length δ_2 is positive, otherwise negative. Analogously, a negative α_2 expresses the fact that the aligned bars $I_{20}B_1$ and $I_{20}A_2$ are pointing to opposite sides. Changing the sign of β_2 means replacing the output angle φ_3 by $\varphi_3 - \pi$. The sign of γ_2 has no influence on the transmission.

Due to (4) the transmission between the angles φ_1, φ_2 and the output angle φ_3 of the second four-bar with $t_3 := \tan\varphi_3/2$ can be expressed by the two biquadratic equations

$$\begin{aligned} c_{22}t_1^2t_2^2 + c_{20}t_1^2 + c_{02}t_2^2 + c_{11}t_1t_2 + c_{00} = 0 \\ d_{22}t_2^2t_3^2 + d_{20}t_2^2 + d_{02}t_3^2 + d_{11}t_2t_3 + d_{00} = 0\,. \end{aligned}$$

The d_{ik} are defined by equations analogue to eqs. (5) and (3). We eliminate t_2 by computing the *resultant* of the two polynomials with respect to t_2 and obtain

$$\det\begin{pmatrix} c_{22}t_1^2 + c_{02} & c_{11}t_1 & c_{20}t_1^2 + c_{00} & 0 \\ 0 & c_{22}t_1^2 + c_{02} & c_{11}t_1 & c_{20}t_1^2 + c_{00} \\ d_{22}t_3^2 + d_{20} & d_{11}t_3 & d_{02}t_3^2 + d_{00} & 0 \\ 0 & d_{22}t_3^2 + d_{20} & d_{11}t_3 & d_{02}t_3^2 + d_{00} \end{pmatrix} = 0\,. \tag{11}$$

This biquartic equation expresses a *4-4-correspondance* between points A_1 and B_2 on the circles a_1 and b_2, respectively.

4. Examples of flexible Kokotsakis meshes

As mentioned above, a continuously flexible Kokotsakis mesh for $n = 4$ is based on a two-fold decomposition of the transmission $\Sigma_1 \to \Sigma_3$ into two spherical four-bars. In view of Fig. 1a we speak of the *right-hand decomposition* via Σ_2 and the *left-hand decomposition* via $\Sigma_4 = \Sigma_2'$. Of course, in the translational type II the two decompositions have identical spherical images.

4.1. Combination of isograms

When two isograms are combined, both 2-2-correspondances split into projectivities $t_1 \mapsto t_2$ and $t_2 \mapsto t_3$ with $0 \mapsto 0$ and $\infty \mapsto \infty$ in the sense of Fig. 3. Hence, also the 4-4-correspondance is composed from such projectivities. Each of them is uniquely defined by any pair $t_1 \mapsto t_3$ with $t_1 \neq 0, \infty$. Beside the two isograms on the right-hand side we can also combine two isograms with lengths $\alpha_1', \ldots, \delta_1'$ on the left-hand side such that both 4-4-correspondances share one projectivity. This proves the continuous flexibility of the *isogonal* type III: Any Kokotsakis mesh consisting of four *isogonal* pyramides — the preimages of spherical isograms — and with any given non-coplanar initial position is continuously flexible (Kokotsakis, 1932).

These arguments are not only true for $n = 4$. We can conclude that — referring to Fig. 1a — for $k \geq 2$ isogonal pyramides on the 'right-hand side' of the central polygon $\mathcal{P}_0$ and $l \geq 1$ isogonal pyramides on the 'left-hand side' with a non-coplanar initial position a flexible Kokotsakis mesh arises with an n-sided central polygon, $n = k + l$. This includes for $n = 3$ the Bricard octahedra of type 3. By (9) we can formulate the closure conditions as

$$\prod_{i=1}^{k} \frac{(\mathrm{s}\alpha_i \pm \mathrm{s}\gamma_i)}{\mathrm{s}(\alpha_i - \gamma_i)} = \prod_{j=1}^{l} \frac{(\mathrm{s}\alpha_j' \pm \mathrm{s}\gamma_j')}{\mathrm{s}(\alpha_j - \gamma_j)} \quad \text{and} \quad \sum_{i=1}^{k} \delta_i = \sum_{j=1}^{l} \delta_j'$$

for any appropriate choice of signs.

4.2. Combination of quadrangles with orthogonal diagonals

In view of Lemma 3 we combine two orthogonal four-bars such that they have one diagonal in common (see Fig. 5a), i.e., under $\alpha_2 = \beta_1$ and $\delta_2 = -\delta_1$, hence $I_{30} = I_{10}$. Then the 4-4-correspondance between A_1 and B_2 is the square of the 2-2-correspondance

$$c_{21} t_1^2 t_3 + c_{12} t_1 t_3^2 + c_{10} t_1 + c_{01} t_3 = 0$$

which expresses the fact that A_1 and B_2 are permanently spherically aligned with I_{20}. The coefficients are

$$\begin{aligned} c_{21} &= \mathrm{t}\beta_2(\mathrm{t}\alpha_1 + \mathrm{t}\delta_1), \quad c_{12} = -\mathrm{t}\alpha_1(\mathrm{t}\beta_2 + \mathrm{t}\delta_1), \\ c_{10} &= \mathrm{t}\alpha_1(\mathrm{t}\beta_2 - \mathrm{t}\delta_1), \quad c_{01} = -\mathrm{t}\beta_2(\mathrm{t}\alpha_1 - \mathrm{t}\delta_1). \end{aligned}$$

Herein t is the abbreviation for the tangent function.

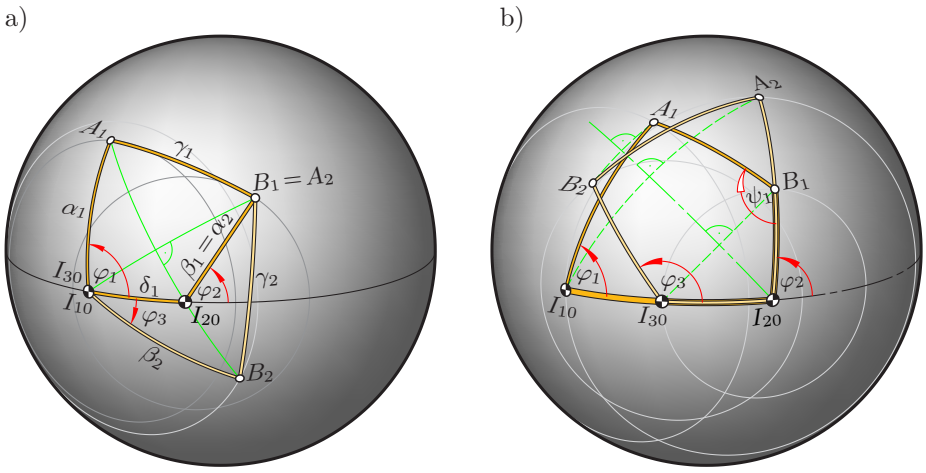

Figure 5: Spherical images of the right-hand decomposition a) of the orthogonal type IV, and b) of the line-symmetric type V

Obviously, any other composition of two such four-bars obeying

$$\mathrm{t}\alpha_1' : \mathrm{t}\delta_1' : \mathrm{t}\beta_2' = \mathrm{t}\alpha_1 : \mathrm{t}\delta_1 : \mathrm{t}\beta_2 \tag{12}$$

gives the same transmission $\varphi_1 \mapsto \varphi_3$. This causes the flexibility of the (3×3)-complexes included in T-nets, first studied in Sauer, Graf (1931). The spherical images of the horizontal folds are located on the great circle $[I_{10}B_1]$, that of the vertical folds on the orthogonal diagonals $[I_{20}A_1]$ or $[I_{20}'A_1']$.

In the following summary we replace the orthogonality-condition (10) by a proportion.

Theorem 4. *Under*

$$\mathrm{c}\alpha_1 : \mathrm{c}\delta_1 : \mathrm{c}\beta_2 = \mathrm{c}\gamma_1 : \mathrm{c}\beta_1 : \mathrm{c}\gamma_2, \quad \alpha_2 = \beta_1 \quad \textit{and} \quad \delta_2 = -\delta_1$$

the transmission $\varphi_1 \mapsto \varphi_3$ (Fig. 5a) depends only on the tangents of α_1, δ_1 and β_2. Hence, any other choice of angles $\alpha_1', \ldots, \delta_2'$ obeying these conditions and eq. (12) gives the same transmission and therefore a flexible Kokotsakis mesh of the orthogonal type IV.

Fig. 6 shows two different decompositions of such a transmission. The underlying overconstrained spherical linkage is a composition of two spherical Dixon-mechanisms (see, e.g., Stachel, 1997). At these mechanisms the bars form a bipartite graph and the knots are moving on two orthogonal great circles.

4.3. A new family of flexible Kokotsakis meshes

Now we specify the second four-bar as mirror of the first one after reflection in an angle bisector at I_{20} (see Fig. 5b). Depending on the choice of the bisector, this implies

$$(\alpha_2,\, \beta_2,\, \gamma_2,\, \delta_2) = (\delta_1,\, \pm\gamma_1,\, |\alpha_1|,\, -\beta_1) \quad \text{or} \quad (-\delta_1,\, \pm\gamma_1,\, |\alpha_1|,\, \beta_1). \tag{13}$$

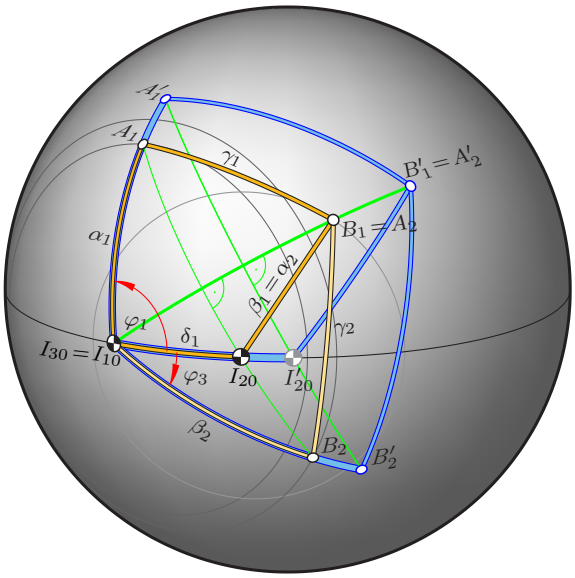

Figure 6: Spherical image of the orthogonal type IV

Angle ψ_1, previously opposite to the input angle φ_1, becomes the output angle, or more precisely, φ_3 equals $\pm\psi_1$ or $\pm(\psi_1 - \pi)$.

However, according to the 4-4-correspondance between A_1 and B_2 there are still two other solutions for φ_3. The corresponding positions of B_2 are mirrors with respect to $[I_{30}A_2]$. Hence, the 4-4-correspondance is reducible, and one component is expressed by eq. (7), i.e., $\mathrm{c}\varphi_3 = \pm(k_1 + l_1\mathrm{c}\varphi_1)$. The sign depends on the choice of the angle bisector at I_{20}.

As already noted in Section 2.2, there are other four-bars with lengths $\alpha'_1, \ldots, \delta'_1$ which produce the same transmission, i.e., with constants $k'_1 = \pm k_1$, $l'_1 = \pm l_1$ by (8) and the same center $I'_{30} = I_{30}$ (Fig. 7). We summarize:

Theorem 5. *For the composition of any four-bar $(\alpha_1, \ldots, \delta_1)$ and its mirror obeying (13) the 4-4-correspondance between A_1 and B_2 splits. For one component the cosines of φ_1 and φ_3 are linearly related. This transmission is shared by other compositions obeying the conditions*

$$\delta_1 + \delta_2 = \delta'_1 + \delta'_2 \pmod{2\pi}$$

and

$$\mathrm{s}\alpha_1\,\mathrm{s}\delta_1 : \mathrm{s}\beta_1\,\mathrm{s}\gamma_1 : (\mathrm{c}\alpha_1\,\mathrm{c}\delta_1 - \mathrm{c}\beta_1\,\mathrm{c}\gamma_1) = \mathrm{s}\alpha'_1\,\mathrm{s}\delta'_1 : \pm\mathrm{s}\beta'_1\,\mathrm{s}\gamma'_1 : (\mathrm{c}\alpha'_1\,\mathrm{c}\delta'_1 - \mathrm{c}\beta'_1\,\mathrm{c}\gamma'_1).$$

The twofold decomposition results in an overconstrained spherical linkage (Fig. 7), which has some properties of so-called *focal mechanisms* in the plane (see, e.g., Wunderlich, 1968). How can the corresponding Kokotsakis mesh be characterized?

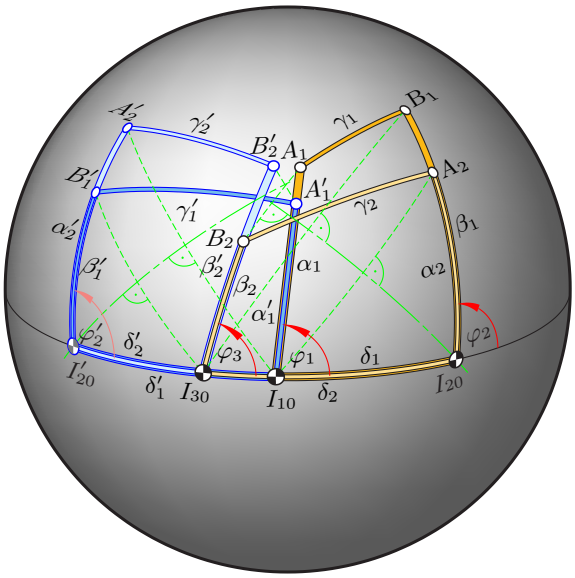

Figure 7: Line-symmetric type V: Two different decompositions of the transmission $\varphi_1 \to \varphi_3$

When at the spherical image the four-bars $I_{10}I_{20}B_1A_1$ and $I_{20}I_{30}B_2A_2$ arise from each other by reflection in an angle-bisector, then the corresponding preimages, the pyramides with apices V_1 and V_2 are symmetric with respect to a line. This axis of symmetry is perpendicular to I_{20} and located in a plane bisecting the adjacent planes in Σ_2 and Σ_0 (compare Fig. 2a). Analogously, the pyramides at V_1' and V_2' are line-symmetric. This is why for this new **type V** the name **line-symmetric** is proposed though the symmetry is not global.

Corollary 6. *A Kokotsakis mesh with mutually line-symmetric pyramides at V_1 and V_2 as well as at V_1' and V_2', which additionally obeys the conditions listed in Theorem 5, is continuosly flexible.*

Kokotsakis' example of a flexible tesselation with convex quadrangles (Kokotsakis, 1932, Fig. 15) is a particular case of this type V, but there also the pyramides at V_1 and V_1' are mutually line-symmetric as well as that at V_2 and V_2' (see Stachel, 2009). Here the signed angles fulfill the following conditions:

$$\alpha_1+\beta_1+\gamma_1+\delta_1=2\pi, \qquad (\alpha_2,\,\beta_2,\,\gamma_2,\,\delta_2)=(-\delta_1,\,\gamma_1,\,\alpha_1,\,\beta_1),$$
$$(\alpha_1',\,\beta_1',\,\gamma_1',\,\delta_1')=(-\delta_1,\,\gamma_1,\,\beta_1,-\alpha_1), \quad (\alpha_2',\,\beta_2',\,\gamma_2',\,\delta_2')=(-\alpha_1,-\beta_1,\,\delta_1,-\gamma_1).$$

The composition of two linear functions of type (7) is still a linear function. Therefore we can iterate and use k pairs of symmetric four-bars on the right-hand side and l pairs on the left-hand side. As long as they share the resulting linear function and the resulting center of rotation, the complete spherical linkage is continuously flexible. The corresponding preimage is a *flexible Kokotsakis mesh* with even $n=2(k+l)$.

Finally is should be mentioned that for given $\alpha_1, \beta_1, \gamma_1, \delta_1$, and β_1' the remaining angles $\alpha_1', \gamma_1', \delta_1'$ obeying the conditions of Theorem 5 can be computed. For β_1' sufficiently close to β_1 real solutions must exist (compare Fig. 7).

References

Bricard, R., 1897. Mémoire sur la théorie de l'octaèdre articulé. J. math. pur. appl., Liouville 3, 113–148.

Bobenko, A.I., Hoffmann, T., Schief, W.K., 2008. On the Integrability of Infinitesimal and Finite Deformations of Polyhedral Surfaces. In: Bobenko et al. (eds.), 2008, Discrete Differential Geometry, Series: Oberwolfach Seminars 38, pp. 67–93.

Karpenkov, O.N., 2008. On the flexibility of Kokotsakis meshes. `arXiv:0812.3050v1[mathDG],16Dec2008`.

Kokotsakis, A., 1932. Über bewegliche Polyeder. Math. Ann. 107, 627–647.

Piekarski, M., 2000. Constructional Solutions for Two-Way-Fold-Deployable Space Trusses. In: Pellegrino, S., Guest, S.D. (eds.), Deployable Structures: Theory and Applications, Kluwer Academic Publ., pp. 301–310.

Pottmann, H., Liu, Y., Wallner, J., Bobenko, A., Wang, W., 2007. Geometry of Multi-layer Freeform Structures for Architecture. ACM Trans. Graphics 26(3), SIGGRAPH 2007.

Sauer, R., 1970. Differenzengeometrie. Springer-Verlag, Berlin/Heidelberg.

Sauer, R., Graf, H., 1931. Über Flächenverbiegung in Analogie zur Verknickung offener Facettenflache. Math. Ann. 105, 499–535.

Stachel, H., 2000. Das Gleichlauf-Kugelgelenk – ein Beispiel zum anwendungsorientierten Unterricht aus Darstellender Geometrie. Proc. SDG Symposium Darstellende Geometrie, Dresden 2000 (ISBN 3-86005-258-6), 151–156.

Stachel, H., 1987. Zur Einzigkeit der Bricardschen Oktaeder. J. Geom. 28, 41–56.

Stachel, H., 1997. Euclidean line geometry and kinematics in the 3-space. In: Artémiadis, N.K., Stephanidis N.K. (eds.): Proc. 4th Internat. Congress of Geometry, Thessaloniki 1996 (ISBN 960-7425-11-1), pp. 380–391.

Stachel, H., 2009. Remarks on Miura-ori, a Japanese Folding Method. Acta Technica Napocensis, Ser. Applied Mathematics and Mechanics 52, Vol. Ia, 245–248.

Wegner, B., 1984. On the projective invariance of shaky structures in Euclidean space. Acta Mech. 53, 163–171.

Wunderlich, W., 1968. On Burmester's focal mechanism and Hart's straight-line motion. J. Mechanism 3, 79–86.